17th World Conference on Earthquake Engineering, 17WCEE
Sendai, Japan - September 13th to 18th 2020

Tests and analysis of small radius curve continuous beam bridges during the Wenchuan Earthquake

D.Z. SUN [1], Y. HUANG [2]
[1] *Institute of Engineering Mechanics, China Earthquake Administration, sundz@iem.ac.cn*
[2] *Institute of Engineering Mechanics, China Earthquake Administration, huangyong@iem.ac.cn*

Abstract

During the Great Wenchuan Ms 8.0 earthquake, many small radius curve continuous beam bridges were damaged on varying degrees, such as Bai-hua Bridge, Hui-lan overpass, Xiao-huan-gou Bridge and so on. The seismic damage phenomenon was classified and summed up. In order to understand the mechanism of the damage, a scaled model was conducted on shaking table. The model was constructed with two span, middle column consolidation and two plate rubber bearing on both ends. Three earthquake ground motions were subjected to the models and the visual results was recorded and seismic damage mechanism was discussed. Then two compared numerical analysis were made, whose differences are the connecting formats of the middle column, one with the beam (A) and the other one with rubber bearing (B). The numerical analysis also affirmed that consolidation of column and beam was not a good connecting format for small radius curve continuous beam bridges.

Keywords: Wenchuan Earthquake, small radius, curve continuous beam bridges

1. Introduction

During the Wenchuan earthquake on May 12, 2008, many continuous girder bridges with small radius suffered different degrees of earthquake damages [1]. For example, Huilan interchange suffered serious damage in Wenchuan earthquake and the failure reason was that shear-bearing capacity of consolidated short columns was insufficient [2].

From the earthquake damage investigation, Baihua bridge with basin type fixed support connection overall collapsed of the curve section. All the xiao-huang-gou middle bridge with single support seriously damaged. Four Yu-zi-xi bridges with basin bearing at middle column and both ends of the column setting basin bearing on one side were seriously affected by landslides. The stiffness of connections from large to small should be: consolidation, basin type fixed bearing, plate type rubber bearing plus anchor bolt, sliding bearing. Different connection ways make the bridges show different stress characteristics under earthquakes.

More researchers have paid attention to the seismic performance of curved bridges through the limited number of shaking table tests and lots of numerical simulations to modeling complicated nonlinear phenomena. Williams performed a series of representational 1/30 scale models to study the effects of both linear and non-linear dynamic behavior, especially for the context of the seismic design of expansion joints [3]. Li Xi presented a comprehensive experimental study of a 1/10 large-scale curved bridge model under multi-support and multi-dimensional excitations [4]. Abdelnaby conducted a hybrid simulation of a curved four-span bridge of different span lengths and unequal column heights. This study has proven that some modeling assumptions widely used in seismic analysis of bridge structures are unrealistic [5].

It is important to study the influence of different substructure forms and different connection ways of substructure on the seismic performance of curved bridges. In this study, one small radius curved bridge was chosen as archetypal structure, and a series of shaking table tests and numerical simulations were performed on a scaled model bridge structure to investigate the seismic damage characteristics.

2. Design of Test

2.1 Test model

A two-span curved bridge with different heights columns was employed, whose superstructure was continuous box girder with 4m of the top, 2.2m of the bottom and 1.4 height. The girder was circular with 20m radius. The columns were 3.43,4.14,4.86, respectively. The middle column was cast-in-place and fixed, while the others was equipped with PTEF slide bearings. The diameter of the column was 800mm, and 20ϕ25 longitudinal bars were evenly arranged along the circumference of the column, with the reinforcement ratio of 1.95% and the stirrup was grade II rebar with diameter of 12mm and stirrup spacing of 100~210mm. However, no obvious stirrup densification area was found in the plastic hinge area, and the calculated volume stirrup ratio was between 0.27%~0.56%.

Then a scaled model with 1/4.706, radius 4.25m was made in order to maximize the use of shaking table. The superstructure was simplified due to lab construction. Model layout and reinforcement are shown in Fig.1 and Fig.2.The fine concrete was used for columns and acceleration magnification was Sa=3. Concrete materials of Ec was1.273×10^4 Mp and the coefficient of stress similarity was Sσ=0.424. Table 1 shows the material information.

© The 17th World Conference on Earthquake Engineering

Table 1-Material Information

Property	Prototype		Model		
	C30	HRB335	Fine concrete	HRB335	HPB235
Modulus of elasticity (GP)	30	200	12.73	200	200
Compressive (yield) strength (MP)	30	335	3.246	335	200

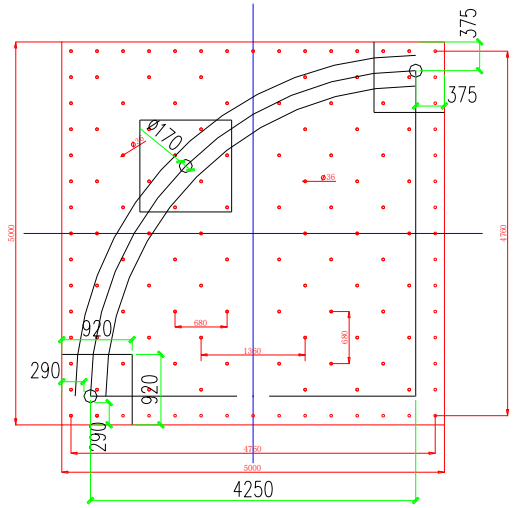

Fig.1 -Model layout diagram

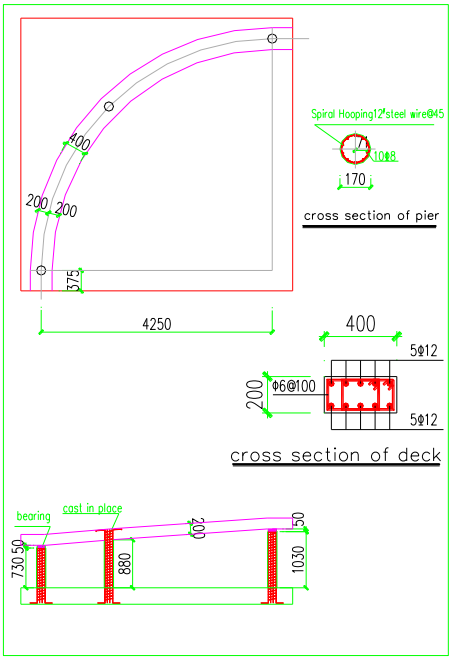

Fig.2- Model reinforcement

It could be seen from the similarity relationship that in order to make the model and the prototype structure meet the similarity relationship, the additional artificial mass of the model structure is needed. Theoretically, the artificial mass should be distributed in each model component. According to the calculation, 22 blocks of 20kg were arranged on the bridge deck.

2.2 Model construction

The model was mainly composed of three parts: bridge deck, column and base. The three parts were bounded with steel bars,respectively, and then cast-in-place concrete, as Fig.3 shown. After the column reinforcement bounded, the strain patches were pasted on both ends of the column to collect the strain changes of the reinforcement.

© The 17th World Conference on Earthquake Engineering

Fig.3- Model construction

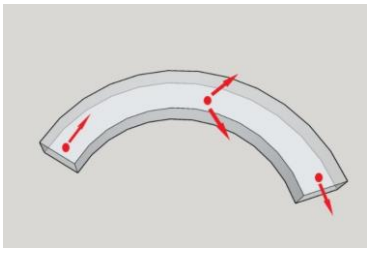

Fig.4- Layout of displacement meter on bridge deck

2.3 Instruments layout

Absolute accelerometer and absolute displacement meter were used in this test. Each column top (actully on the deck) was equipped with accelerometers in three directions, and the arrangement of displacement meters were shown in the Fig. 4 and table 2.

Table 2- Instruments layout summary

	Displacement meter	**Accelerometer**
Table top	2	3
Column	6	0
Deck	4	9
Total	12	12

For the selection of seismic motion, El Centro wave and Taft wave were selected due to the influence of table displacement limitation. The ratio of peak acceleration in three directions was 1:0.85:0.65. The test cases for the shaking table were shown in Table 3.

Table 3 - Test cases for the shaking table

			Ground motion input		
			X(g)	**Y(g)**	**Z(g)**
1	Flat noise		0.05	0.05	0.05
2	7th degree frequent earthquake （E1）	Taft	0.165	0.14	0.107
3			0.14	0.165	0.107
4		EICentro	0.165	0.14	0.107
5			0.14	0.165	0.107
6	Flat noise		0.05	0.05	0.05
7	7th degree basic earthquake	Taft	0.45	0.383	0.293
8			0.383	0.45	0.293
9		EICentro	0.45	0.383	0.293
10			0.383	0.45	0.293

© The 17th World Conference on Earthquake Engineering

11	Flat noise		0.05	0.05	0.05
12	7th degree rare earthquake （E2）	Taft	0.93	0.79	0.605
13			0.79	0.93	0.605
14		EICentro	0.93	0.79	0.605
15			0.79	0.93	0.605
16	Flat noise		0.05	0.05	0.05
17	8th degree rare earthquake	Taft	1.20	1.02	0.78
18			1.02	1.20	0.78
19		EICentro	----	-----	------
21			1.02	1.20	0.78
22	Flat noise		0.05	0.05	0.05

3. Analysis

3.1 Phenomenon analysis

Under frequent seismic inputs, namely 7-degree earthquake intensity (E1), no visible cracks and no obvious change of the structure were found.

Under basic seismic inputs, the cracks began to happen. Under Taft wave with Y direction 0.45g, circumferential fine cracks appearred at the top of the middle column, with a length of about 20cm, and circumferential cracks to the top of the syncline at the bottom of the column, with a length of about 6cm, shown as Fig.5.

Fig.5 - circumferential fine cracks under taft wave with Y direction 0.45g

Then the cracks continued to develop and new circumferential cracks appeared at the bottom of the column, with a length of about 5cm. At the height of 1 / 5 from the top of the column, there were circumferential and diagonal cracks, the length of which was about 25cm, shown as Fig.6.The circumferential cracks were mainly caused by torsion, while the diagonal parts were caused by shear force At the same time, the sliding amount of the top support of the two ends of the column was about 5mm, and the trend of increasing the sliding was not obvious.

© The 17th World Conference on Earthquake Engineering

Fig.6 -Circumferential and diagonal cracks

Fig.7- final status of the middle column

Under Rare earthquake inputs, Taft wave with Y direction 0.93g, from the top of the middle column, there was a diagonal downward crack with a length of about 40 cm, and another vertical crack which was approximately parallel to it. At the bottom of the crack, a circumferential crack with a length of about 10 cm apperred. On the other side of the column, there were several inclined vertical cracks, all of which were about 5cm long. New circumferential cracks appearred at the bottom of column. The concrete was crushed from the top 8 cm and the bottom 8 cm of the middle column. At the same time, the sliding amount of the bearing at the top of the two ends of the columns increased to about 1cm, and the bearing of the short column slided along the 45 degree angle.

When the earthquake motion of the table rised to 1.45g, the concrete at both ends of the middle column was crushed seriously, the cracks connected with each other, and the slip at both columns increased to 2cm.

From 0.45g input, circumferential cracks appeared at both ends of the column, which mainly were caused by the clockwise torque. With the increase of PGA inputs, the torque gradually increased, and the crack length also widened and lengthened. When PGA reached 0.8g, diagonal cracks began to appear. The diagonal cracks were the result of multiple actions of compression, bending and torsion. When PGA reached 1.45g, the concrete crushed. According to the location of the final crack and the concrete compression phenomenon, it was in good agreement with the actual earthquake damage. The basic frequency changes of model were shown in Table 4.

Table 4- Basic frequency changes of model

Seismic inputs	Direction	Frequency (HZ)	Period(s)
Before 7th degree frequent earthquake inputs	X	6.13	0.163
	Y	6.15	0.163
After 7th degree basic earthhquake inputs	X	6.2	0.161
	Y	6.2	0.161

The model was basically in good condition before 7th degree frequent earthquake inputs. The model appearred to be damaged from 7th degree basic earthhquake inputs. After rare earthquake inputs, there was a large damage, even concrete crushing under 8th degree rare earthquake inputs.

© The 17th World Conference on Earthquake Engineering

However, due to the basically intact columns on both sides and the isolation effect of rubber bearings, the period after damage was basically unchanged. Fig.8 and Fig.9 were the accelerations and displacements of middle column top under Taft wave with Y direction 0.93g. Fig.10 and and Fig.11 were the accelerations and displacements of middle column top under Taft wave with Y direction 1.2g.

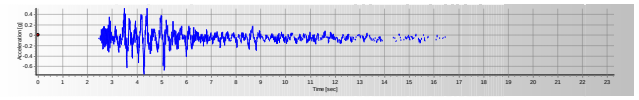

(x)

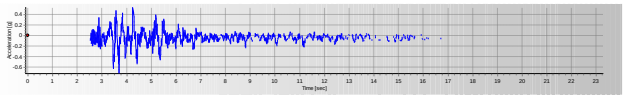

(y)

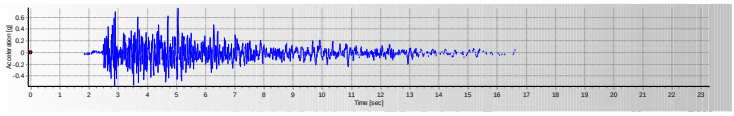

(z)

Fig.8-The accelerations of middle column top under Taft wave with Y direction 0.93g

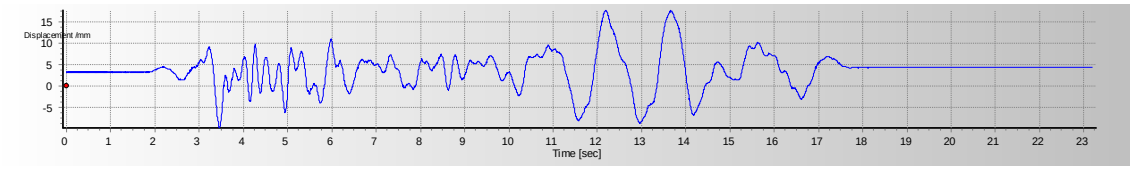

(x)

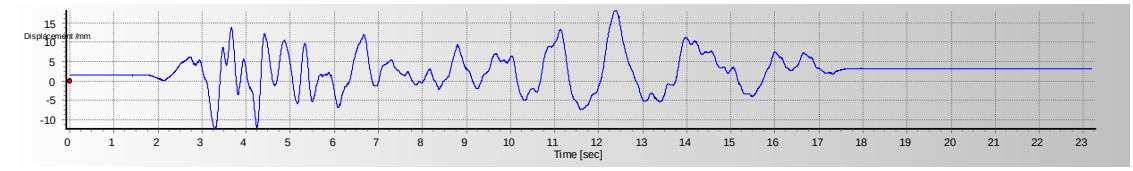

(y)

Fig.9- The displacements of middle column top under Taft wave with Y direction 0.93g

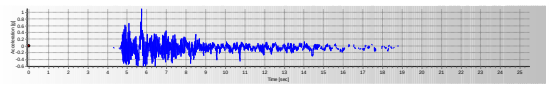

(x)

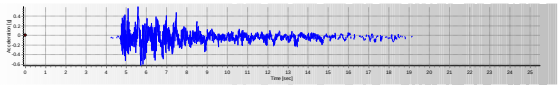

(y)

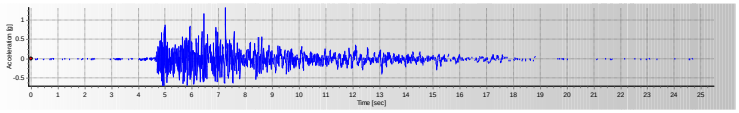

(z)

Fig.10-The accelerations of middle column top under Taft wave with Y direction 1.2g

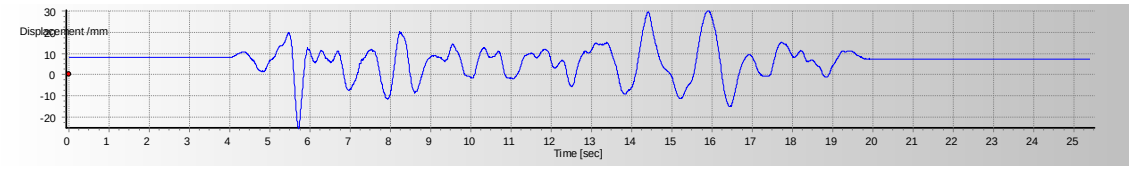

(x)

© The 17th World Conference on Earthquake Engineering

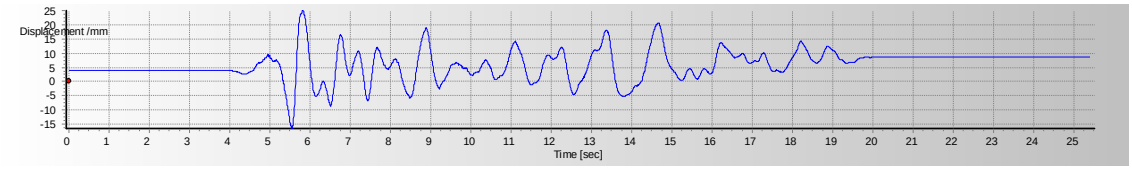

(y)

Fig.11- The displacements of middle column top under Taft wave with Y direction 1.2g

3.2 Numerical analysis

The finite element model of seismic response analysis of curved continuous girder bridge was established by MIDAS/Civil. The girder and column were connected by spatial beam and pole element. The bearing was connected by master-slave node, and the three-way spring stiffness was set according to the seismic rules. There were 113 beam elements and 120 nodes in the finite element model of the whole bridge, which was in Fig.12. The top of two side columns adoptted two-way movable bearing, and the middle columns were compared according to two working conditions of consolidation and fixed bearing. Number 1,2,3 was set from low column to high column.

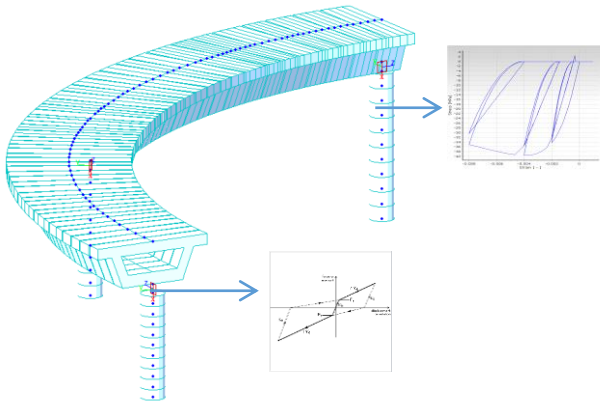

Fig.12 The finite element model

The strong earthquake records of ba-jiao and Qing-ping stations of Wenchuan earthquake were used as three-dimensional seismic inputs, shown in Fig.13 and 14.

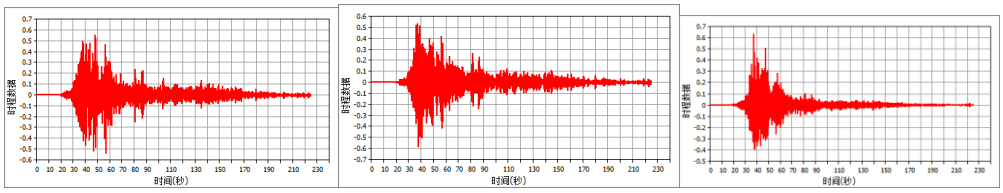

Fig.13-Acceleration time history curves of ba-jiao station（EW、NS、UD）

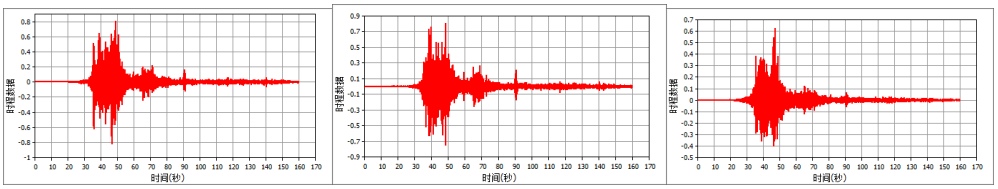

Fig.14-Acceleration time history curves of qing-ping station（EW、NS、UD）

© The 17th World Conference on Earthquake Engineering

In order to check the internal forces of columns of curved continuous girder bridge, the maximum internal forces at several key points were output, and the calculation results were shown as belows.

Table 5-The maximum internal force at the bottom of column when middle column fixed

Strong earthquake records	position	Axial force (kN)	Shear-y (kN)	Shear-z (kN)	Torque (kN*m)	Bending moment-y (kN*m)	Bending moment -z (kN*m)
Ba-jiao	No.1 column botom	610.18	7.32	845.6	119.18	85.35	500.00
	No.2 column botom	1254.24	1289.08	901.63	84.59	94.88	1377.73
	No.3 column botom	440.230	1020.23	10.73	75.09	70.00	592.69
Qing-ping	No.1 column botom	613.25	-29.12	775.27	101.84	97.85	409.00
	No.2 column botom	1134.82	1226.54	1132.64	77.51	148.42	1128.85
	No.3 column botom	455.84	840.15	39.01	80.25	27.19	632.74

Maximum absolute displacements of column top in seismic response was shown in Table 6.

Table 6- Maximum absolute displacement of column top(mm)

Strong earthquake records	No.1 column top (X diretion)	No.2 column top (X diretion)	No.3 column top (X diretion)	No.1 column top (Y diretion)	No.2 column top (Y diretion)	No.3 column top (Y diretion)
Ba-jiao	54	79	0.9	0.2	115	128
Qing-ping	30	58	3	0.9	61	67

Table 7 showed the maximum value of absolute accelerations under the seismic action of each column.

Table 7 -The maximum value of absolute accelerations(mm/s^2)

Strong earthquake records	No.1 column top (X diretion)	No.2 column top (X diretion)	No.3 column top (X diretion)	No.1 column top (Y diretion)	No.2 column top (Y diretion)	No.3 column top (Y diretion)	No.1 column top (Z diretion)	No.2 column top (Z diretion)	No.3 column top (Z diretion)
Ba-jiao	23300	17135	7784	6182	22085	30750	6744	8297	6919
Qing-ping	21726	15156	28110	35280	17205	32482	57098	5838	6130

© The 17th World Conference on Earthquake Engineering

Table 8- The maximum internal force of the column bottom when the middle column is fixed with support

Strong earthquake records	position	Axial force	Strong earthquake records	position	Axial force	Strong earthquake records	position
Ba-jiao	**No.1 column botom**	-249.92	-3.83	301.27	93.00	-63.80	369.96
	No.2 column botom	567.36	-640.81	656.26	69.53	-125.04	1253.18
	No.3 column botom	255.75	351.08	5.62	-51.47	-47.26	-405.54
Qing-ping	**No.1 column botom**	-195.22	-12.32	-251.57	125.35	37.38	129.20
	No.2 column botom	-537.83	561.08	556.70	110.75	-101.41	-1014.8
	No.3 column botom	168.51	-227.39	-16.50	89.29	135.97	208.58

Table 9- Maximum absolute displacement of column top when the middle column is fixed with support (mm)

Strong earthquake records	No.1 column top (X diretion)	No.2 column top (X diretion)	No.3 column top (X diretion)	No.1 column top (Y diretion)	No.2 column top (Y diretion)	No.3 column top (Y diretion)
Ba-jiao	42	99	0.9	0.2	102	91
Qing-ping	23	90	3	0.9	89	45

Table 10 -The maximum value of absolute accelerations when the middle column is fixed with support (mm/s^2)

Strong earthquake records	No.1 column top (X diretion)	No.2 column top (X diretion)	No.3 column top (X diretion)	No.1 column top (Y diretion)	No.2 column top (Y diretion)	No.3 column top (Y diretion)	No.1 column top (Z diretion)	No.2 column top (Z diretion)	No.3 column top (Z diretion)
Ba-jiao	17918	22773	7784	6182	21913	27996	6676	7726	6822
Qing-ping	20849	16770	28110	35280	18457	24032	5606	5686	6082

Under the action of gravity load, the axial force of No. 2 column was about 1000kN and the yield moment was about 1284kN·m. Assuming that the reverse bending point located in the middle of the column span, the corresponding yield shear force was 948kN. According to the relationship

© The 17th World Conference on Earthquake Engineering

between the shear strength and the displacement ductility coefficient calculated by priestiey formula, when the displacement ductility coefficient was less than 2, the full section of the column concrete participates in the shear resistance, and its value was 1200kN, which was greater than the corresponding shear force 948kN when the column was bent and yielding, and the column would occur bending and yielding. After that, with the increase of displacement ductility, the concrete would gradually withdraw from the shear resistance due to crack development and other factors, and the column The shear strength would be reduced to below 800kN, at this time, the column will have shear failure.

Therefore, based on the above analysis, it was believed that the bending yield of No. 2 column occurred firstly in the earthquake excitations, and then the shear contribution of concrete decreased due to the development of concrete cracks, and finally shear failure occurred due to the lack of shear capacity.

From the calculation results, it could be found that although the structural resistance increases correspondingly in the case of consolidation, the bending moment and shear force were relatively larger, and close to the yield shear force at 0.2g. Therefore, the case of consolidation was more likely to be damaged. However, the shear force of the fixed bearing was only 60-70 percent of its yielded capacity. Therefore, the shear force of the structure was reduced under the case of the fixed bearing, but the displacement of the top was increased correspondingly. Therefore, the selection of the structure type needed to consider the corresponding indicators comprehensively.

4. Acknowledgements

This study is funded by National Natural Science Fund of China (NSFC) (Grant No. 51678544). The results and conclusions presented in the paper are related to the authors and do not necessarily reflect the view of the sponsors.

5. Copyrights

17WCEE-IAEE 2020 reserves the copyright for the published proceedings. Authors will have the right to use content of the published paper in part or in full for their own work. Authors who use previously published data and illustrations must acknowledge the source in the figure captions.

6. References

[1] Qiang Han, Xiuli Du, Jingbo Liu, et al. Seismic damage of highway bridges during the 2008 Wenchuan earthquake. *Earthq Eng Eng Vib* 2009;8(2):263–73.

[2] Wang Dongsheng, Sun Zhiguo, Li Xiaoli, et al. Seismic damage investigation and failure mechanism analysis of curved bridges in Wenchuan earthquake, 2010; 30(5): 572–579 (in Chinese)

[3] Williams D, Godden W. Seismic response of long curved bridge structures: experimental model studies. *Earthq Eng Struct Dyn* 1979;7(2):107–28.

[4] Xi Li, Deyi Zhang, Weiming Yan, et al. Shake-table test for a typical curved bridge: wave passage and local site effects. *J Bridge Eng* 2015;20(2):1–14.

[5] Abdelnaby Adel E, Frankie Thomas M, Elnashai Amr S, et al. Numerical and hybrid analysis of a curved bridge and methods of numerical calibration. *Eng Struct* 2014;70(70):234–45.

© The 17th World Conference on Earthquake Engineering